ACS APPLIED MATERIALS & INTERFACES

Research Article

www.acsami.org

# Synthesis of a Low-Bandgap Fluorinated Donor–Acceptor Copolymer and Its Optoelectronic Application

Hui-Jun Yun,[†] Moon Chan Hwang,[†] So Min Park,[†] Ran Kim,[§] Dae Sung Chung,*[,‡] Yun-Hi Kim,*[,§] and Soon-Ki Kwon*[,†]

[†]School of Nano & Advanced Materials Science and Engineering and ERI, Gyeongsang National University, Jinju, 660-701, Korea

[§]Department of Chemistry and Research Institute of Natural Science (RINS), Gyeongsang National University, Jinju, South Korea 660-701

[‡]School of Chemical Engineering and Material Science, Chung-Ang University, Seoul 156-756, South Korea

Supporting Information

**ABSTRACT:** We demonstrate the synthesis of a new copolymer which is composed of dialkyl thienylated benzodithiophene and perfluororalkyl-carbonyl thienothiophene (DTBDT-TTFO) and the characterization of its optoelectronic properties. The introduction of thienyl groups enabled the extended delocalization of $\pi$ electrons in the DTBDT-TTFO backbone and efficient intermolecular charge transport as proved by the fairly high field effect mobility of 0.02 $cm^2/(V\ s)$. The introduction of perfluororalkyl-carbonyl side chains resulted in a significant red-shift of DTBDT-TTFO in the absorption spectra and a decrease in the HOMO and LUMO levels. The resulting energy levels of DTBDT-TTFO were not satisfactory for solar cell applications, especially in terms of charge separation at the polymer/PCBM interfaces. Rather, the DTBDT-TTFO showed better energy level matching with the colloidal nanocrystals (NCs) of CdSe. A photodetector based on the bulkheterojunction of DTBDT-TTFO and CdSe NCs with coplanar device geometry resulted in a high photoconductive gain (responsivity higher than 1A/W under a low operating voltage of 1 V), possibly arising from electron trapping at CdSe NCs such that the hole can travel along the detector and its surrounding circuit. More importantly, the photodetector revealed a time constant of a few hundreds of microseconds, which means that the response speed of the photodetector is fast enough for lag-free imaging applications.

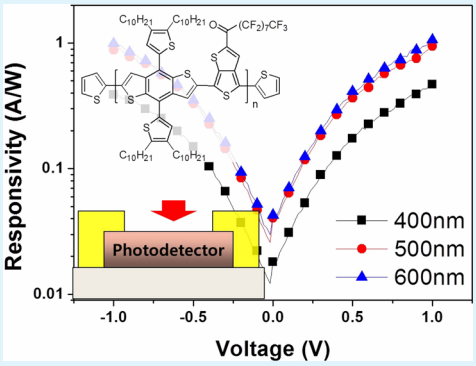


**KEYWORDS:** *polymer, semiconductor, PBDTTT, photodetector, mobility, nanocrystal*

## INTRODUCTION

Conjugated polymers have attracted much attention because their processability and physicochemical properties can be easily tuned.[1−5] Together with other potential advantages such as their low cost, lightweight and flexibility, such chemically tunable characteristics mean that conjugated polymers are the most desirable materials for many opto-electronic applications. For example, poly(3-hexylthiophene) (P3HT), which can form a well-aligned intermolecular $\pi$-stacking structure in a thin film state, shows very successful charge transport behavior with a charge carrier mobility of 0.1 $cm^2/(V\ s)$ when fabricated as an organic thin film transistor (OTFT).[6−8] Accordingly, numerous attempts have been made to tune the chemical structure of P3HT in an effort to enhance the charge transport behavior of conjugated polymers. Among the many successful post-P3HT polymers, the most widely known examples are poly(3,3‴-didodecyl quaterthiophene) (PQT-12),[9] poly(2,5-bis(3-alkylthiophene-2-yl)thieno[3,2-b]thiophene) (PBTTT),[10] and the very recently reported diketopyrrolopyrrole (DPP)-based copolymers.[11−13] These polymers have either more efficient $\pi$-stacking structure (PQT-12 and PBTTT) or more efficient intermolecular overlap of their electronic wave functions (DPP-based copolymers) compared to P3HT, both resulting in much higher charge carrier mobility than P3HT.

In organic photovoltaic applications, (OPVs) a bulk heterojunction (BHJ) consisting of P3HT and PCBM was the first generation of materials for use in high performance OPVs. After significant research efforts to optimize the donor–acceptor interaction, the morphology of the composite films, the interfacial properties, and the device structure, the power conversion efficieny (PCE) reached as high as 5%.[14−16] Therefore, to enhace the photovoltaic properties of such BHJ based OPVs further, several new polymers have been synthesized by modifying the chemical structure of P3HT. In general, the synthetic strategies used to enhance the PCE in those polymers involved reducing the bandgap and lowering the highest occupied molecular orbital (HOMO) level to increase light harvesting and the open circuit voltage,

Received: March 2, 2013
Accepted: June 17, 2013
Published: June 17, 2013

   dx.doi.org/10.1021/am4007935 | ACS Appl. Mater. Interfaces 2013, 5, 6045−6053

respectively. The most successful examples of these approaches were poly[2,6-(4,4-bis-(2-ethylhexyl)-4H-cyclopenta [2,1-b;3,4-b′]-dithiophene)-*alt*-4,7-(2,1,3-benzothiadiazole)] (PCPDTBT)[17] and poly[4,8-bis-substituted-benzo[1,2-b:4,5-b′]dithiophene-2,6-diyl-*alt*-4-substituted-thieno[3,4-b]-thiophene-2,6-diyl] (PBDTTT),[18−22] enabling high PCE of the resulting OPVs that exceeded 8%. Morphology is another critical factor in BHJ based OPVs. It is known that the donor and acceptor domains should be twice the size of the exciton diffusion length (∼10 nm) to build up bicontinuous interpenetration network.[23] Thermal annealing[24] and solvent annealing[25] are currently the most efficient way for such optimized morphology. Charge extraction at organic-electrode interface is also a limiting factor for OPV performance.[26] The insertion of appropriated interface layer can reduce the energy barrier between the orgainc layer and electrode, thus accelerating charge extraction. They can also provide selective extraction for single type of carriers, such as $TiO_x$[27] or ZnO,[28] which serves both as an electron transporting layer and as a hole-blocking layer.

Although the progress in the area of polymer semiconductors has been impressive, there is still much to do before the realization of practical polymer-based optoelectronic devices. Here we synthesized a new PBDTTT derivative, DTBDT-TTFO, for high performance optoelectronic applications (Scheme 1). A thienyl-substituted benzodithiophene core is introduced to broaden the absorption capability of polymers. It is widely known that such side chain-conjugated polymers possess higher hole mobility thanks to the 2-D conjugation structure of polymer backbone.[19] Moreover, dialkyl groups in the thienyl provide good solubility of the polymer, enabling the creation of a high quality thin film via a solution process. Perfluoroalkyl carbonyl-substituted thieno-[3,4-b]thiophene is also introduced to enhance intermolecular interaction of the resulting polymers, as fluorine can form numerous secondary bonds with other molecules. In addition, the introduction of fluorine, an atom of high electron affinity, can lower the HOMO level of the resulting polymer, leading to an increase in $V_{OC}$ when fabricated as OPVs.[20,21] With these factors in mind, we demonstrate in this study various electronic and optoelectronic applications of DTBDT-TTFO, including OTFTs with a charge carrier mobility of 0.02 $cm^2/(V\ s)$, OPVs with a $V_{OC}$ of 0.8 V and organic photodetectors (OPD) with a high responsivity value of 1 A/W. The photophysical origins behind such performances are fully discussed and described with various characterization tools.

## EXPERIEMENTAL SECTION

**Synthesis of Polymer.** All chemical reagents were purchased from Aldrich and used as received. Pd catalysts were purchased from Strem Chemicals Inc. The other materials were common commercial level and used as received. All solvents used were further purified prior to use.

*4-Bromothiophene-3-carbaldehyde (**1**).* The synthetic details can be found in the previous report.[29] Yield: 34.3 g (87%). $^1$H NMR (300 MHz, $CDCl_3$): $\delta$ = 9.95 (s, 1H), 8.16 (d, 1H), 7.37 (d, 1H). $^{13}$C NMR (75 MHz, $CDCl_3$): $\delta$ = 185.3, 145.6, 139.2, 128.4, 111.7. EI, MS *m*/*z*: 191 (M+).

*Ethyl Thieno[3,4-b]thiophene-2-carboxylate (**2**).* The synthetic details can be found in the previous report.[29] Yield: 23.4 g (62%). $^1$H NMR (300 MHz, $CDCl_3$): $\delta$ 7.72 (s, 1H), 7.76 (d, 1H), 7.31 (d, 1H), 4.43 (m, 2H), 1.43 (t, 3H). $^{13}$C NMR (75 MHz, $CDCl_3$): $\delta$ = 175.7, 147.6, 146.6, 137.2, 131.0, 102.8, 100.3, 23.1, 14.4. EI, MS *m*/*z*: 219.2 (M+).

*Thieno[3,4-b]thiophen-2-ylmethanol (**3**).* The synthetic details can be found in the previous report.[29] Yield: 15.7 g (85%). $^1$H NMR (300 MHz, $CDCl_3$): $\delta$ = 7.26 (d, 1H), 7.21 (d, 1H), 6.81 (s, 1H), 4.75 (s, 2H), 2.39 (s, 1H (−OH)). $^{13}$C NMR (75 MHz, $CDCl_3$): $\delta$ = 175.6, 146.8, 145.4, 137.2, 131.2, 102.8, 100.3, 25.1. EI, MS *m*/*z*: 170.2 (M+).

*Thieno[3,4-b]thiophene-2-carbaldehyde (**4**).* The synthetic details can be found in the previous report.[29] Yield: 6.4 g (43%). $^1$H NMR (300 MHz, $CDCl_3$): $\delta$ = 10.01 (s, 1H), 7.78 (d, 1H), 7.69 (s, 1H), 7.35 (d, 1H). $^{13}$C NMR (75 MHz, $CDCl_3$): $\delta$ = 185.5, 149.7, 145.6, 139.3, 128.0, 118.9, 111.8. EI, MS *m*/*z*: 168.2 (M+).

*2,2,3,3,4,4,5,5,6,6,7,7,8,8,9,9,9-Heptadecafluoro-1-(thieno[3,4-b]-thiophen-2-yl)nonan-1-ol (**5**).* Under the protection of nitrogen, MeLi (10.2 mL, 0.016 mol, 1.6 M solution) was added dropwise to thieno[3,4-b]thiophene-2-carbaldehyde (2.5 g, 0.0149 mol) in ether (75 mL) at −78 °C and stirred for 40 min. Then perfluorooctyliode (10.7 g, 0.020 mol) was slowly added at −78 °C. After 6 h, the reaction was stopped and water (100 mL) was added, and then the mixture was extracted by diethyl ether twice. After removing the solvent, it was dissolved in dried $CH_2Cl_2$. This material is sufficiently pure to use for the next synthetic step. Yield: 4.2 g (48%). $^1$H NMR (300 MHz, $CDCl_3$): $\delta$ = 7.42 (s, 1H), 7.29 (s, 1H), 7.09 (s, 1H), 5.42 (m, 1H), 2.81 (s, 1H(−OH)). $^{19}$F (500 MHz, $CDCl_3$): $\delta$ = −82.13 (3F), −144.53 (2F), −122.17 (4F), −122.03 (4F), −123.04 (2F), −126.47 (2F). EI, MS *m*/*z*: 588.3 (M+).

*2,2,3,3,4,4,5,5,6,6,7,7,8,8,9,9,9-Heptadecafluoro-1-(thieno[3,4-b]-thiophen-2-yl)nonan-1-one (**6**).* A solution of compound **5** (4.2 g, 7.1 mmol) in $CH_2Cl_2$ (100 mL) and activated $MnO_2$ (0.9 g, 10.7 mmol) was stirred overnight. The mixture was then filtered through Celite. The filtrate was dried over $MgSO_4$ and filtered, and the solvent was evaporated in vacuum to afford the crude product. Yield: 4.0 g (96%). $^1$H NMR (300 MHz, $CDCl_3$): $\delta$ = 7.95 (s, 1H), 7.92 (s, 1H), 7.38 (s, 1H). $^{19}$F NMR (500 MHz, $CDCl_3$): $\delta$ = −81.13 (3F), −144.52 (2F), −121.47 (4F), −122.02 (4F), −123.06 (2F), −126.49 (2F). EI, MS *m*/*z*: 586.29 (M+).

*1-(4,6-Dibromothieno[2,3-c]thiophen-2-yl)-2,2,3,3,4,4,5,5,6,6,7,7,8,8,9,9,9-heptadecafluorononan-1-one (TTFO) (**7**).*[29,30] A solution of compound 6 (4.0 g, 6.8 mmol) in DMF and protected from light was cooled to 0 °C. *N*-Bromosuccinimide (3.0 g, 17.1 mmol) was added in small portions over 15 min, and then the reaction was stirred for 3 h. The mixture was poured into water (100 mL) and was extracted with ether. The organic layer was dried over anhydrous $MgSO_4$, and the solvent was removed by rotary evaporation. The residue was purified by column chromatography and purified by crystallization from ether/ethanol to yield compound 7 as a needle shaped brown solid. Yield: 4.1 g (81%). mp: 140 °C. $^1$H NMR (300 MHz, $CDCl_3$): $\delta$ = 7.72 (s, 1H). $^{19}$F NMR (500 MHz, $CDCl_3$): $\delta$ = −81.14 (3F), −144.54 (2F), −121.49 (4F), −122.09 (4F), −123.07 (2F), −126.48 (2F). FT-IR (KBr) ($cm^{-1}$): 3115 (aromatic), 1680 (C═O), 1200−1100 (−C−C−). HRMS (EI+) *m*/*z* calcd for ($C_{15}HBr_2F_{17}OS_2$), 741.7564; found, 741.7563 ($M^+$).

*4,8-Bis(2,3-didecylthiophene)-benzo-[1,2-b:4,5-b′]dithiophene (**8**).* Under the protection of nitrogen, *n*-butyllithium (5.43 mL, 13.6 mmol, 2.5 M solution in hexane) was added dropwise to 2,3-didecylthiophene (4.5 g, 12.4 mmol) in THF (40 mL) at 0 °C. Further details can be found in the previous report.[31] Yield: 2.5 g (47%). $^1$H NMR (300 MHz, $CDCl_3$): $\delta$ = 7.69 (d, 2H), 7.46 (d, 2H), 7.23 (s, 2H), 2.85 (t, 4H), 2.62 (t, 4H), 1.72 (m, 8H), 1.30 (m, 56H), 0.90 (t, 12H). $^{13}$C NMR (75 MHz, $CDCl_3$): $\delta$ = 140.18, 138.86, 138.09, 136.36, 135.08, 129.85, 127.23, 124.14, 123.56, 31.92, 30.79, 29.64, 29.62, 29.60, 29.55, 29.49, 29.43, 29.34, 28.31, 28.00, 22.68, 14.07. EI, MS *m*/*z*: 915.60 (M+).

*2,6-Bis(trimethyltin)-4,8-bis(2,3-didecylthiophene)-benzo-[1,2-b:4,5-b′]dithiophene (DTBDT) (**9**).* Under the protection of nitrogen, *n*-butyllithium (2.5 mL, 5.0 mmol, 2.0 M solution in cyclohexane) was added dropwise to 4,8-bis(2,3-didecylthiophene)-benzo-[1,2-b:4,5-b′]dithiophene (2.0 g, 2.2 mmol) in THF (40 mL) at room temperature and stirred for 2 h at 50 °C. Then trimethyltin chloride (5.5 mL, 5.5 mmol, 1.0 M in hexane) was added in one portion at room temperature. After 6 h, the reaction was stopped and water (100 mL) was added, and then the mixture was extracted by diethyl ether

**Scheme 1. Synthesis of Monomers and Polymer**

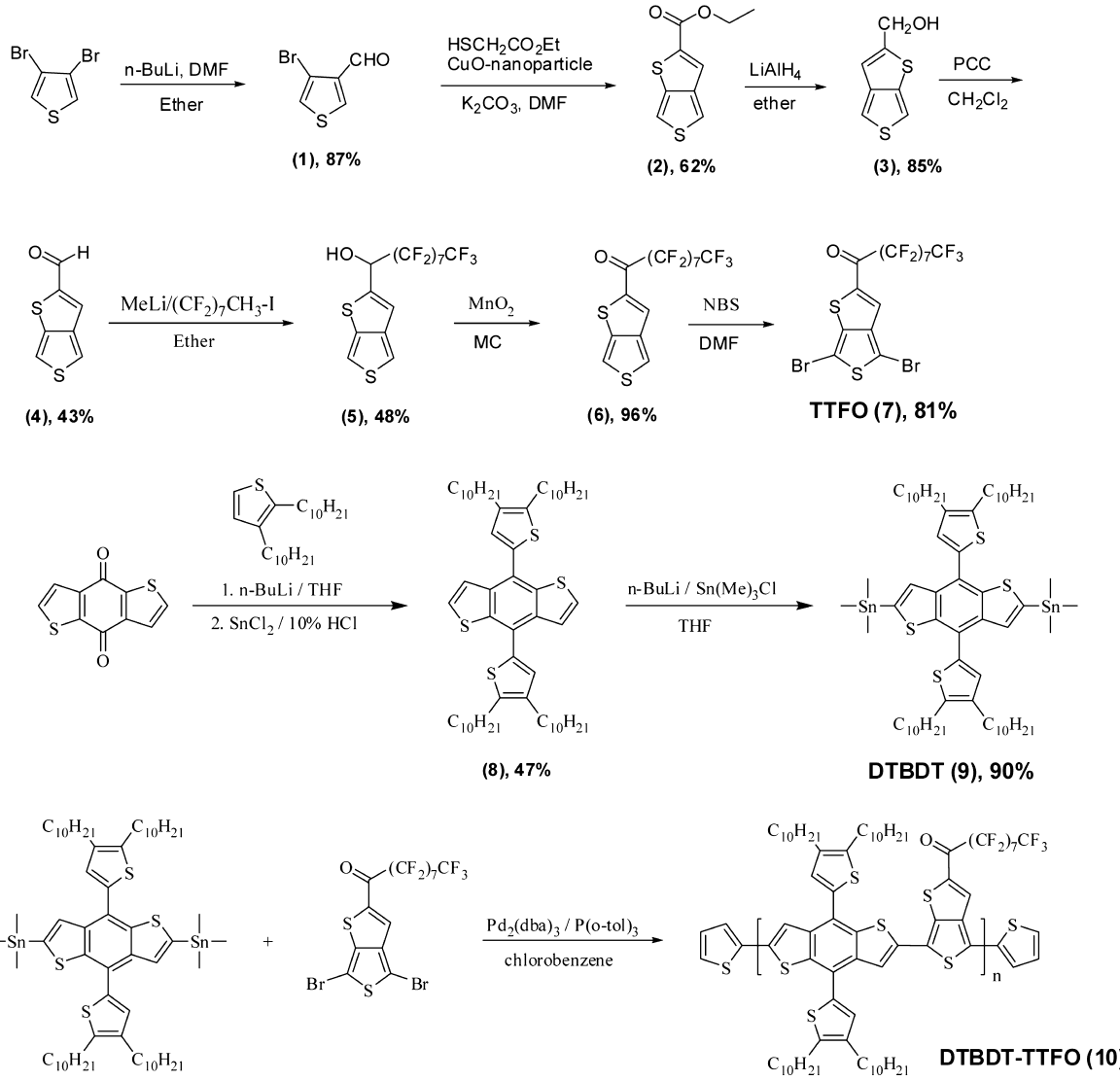


twice. After removing the solvent, the residue was purified by recrystallization from ether/ethanol (1:5). Yield: 2.45 g (90%). mp: 76.5 °C. $^1$H NMR (300 MHz, $CDCl_3$): $\delta$ = 7.74 (s, 2H), 7.24 (s, 2H), 2.85 (t, 4H), 2.63 (t, 4H), 1.70 (m, 8H), 1.29 (m, 56H), 0.90 (t, 12H), 0.41 (t, 18H). $^{13}$C NMR (75 MHz, $CDCl_3$): $\delta$ = 141.88, 139.78, 137.97, 137.20, 135.78, 131.41, 129.81, 122.50, 31.91, 31.82, 30.82, 29.69, 29.66, 29.64, 29.53, 29.49, 29.35, 28.33, 28.02, 22.68, 14.07, 8.39. FT-IR (KBr) ($cm^{-1}$): 3108 (aromatic), 2923−2855 (aliphatic, C−H). EI, MS *m*/*z*: 1241.2 (M+).

*Poly{4,8-bis(2,3-didecylthiophene)-benzo-[1,2-b:4,5-b′]-dithiophene-5,5′-diyl-alt- 2,2,3,3,4,4,5,5,6,6,7,7,8,8,9,9,9-heptadeca-fluoro-1-(thieno[3,4-b]thiophen-2-yl)nonan-1-one-1,5-diyl} (DTBDT-TTFO) (**10**).* Compound **9** (0.5000 g, 0.403 mmol) and compound 7 (0.2997 g, 0.403 mmol) were dissolved into 5 mL of chlorobenzene in a flask protected by nitrogen. The solution was flushed with high purity nitrogen for 30 min, and then $Pd_2(dba)_3$ (7.3 mg, 0.008 mmol) and $P(o\text{-}tol)_3$ (9.7 mg, 0.032 mmol) were added into the flask. The sand bath was gradually heated to 110 °C, and the reactant was stirred for 48 h at 110 °C under high purity nitrogen atmosphere. Then, the reaction mixture was cooled down to room temperature and polymer was precipitated by addition of 100 mL of methanol, and the solid was washed with MeOH, acetone, hexane, and chloroform in a Soxhlet apparatus. After the chloroform solution was concentrated and then added dropwise into methanol, the pure polymer was dried. Yield: 0.48 g (80%). $^1$H NMR (500 MHz, $CDCl_3$): $\delta$ = 8.21−6.83 (br, 5H), 2.79−2.57 (br d, 8H), 1.69−1.62 (br d, 8H), 1.25−1.19 (br, 56H), 0.81−0.93 (br s, 12H). FT-IR (KBr) ($cm^{-1}$): 3081 (aromatic), 2923−2850 (aliphatic, C−H), 1687 (C═O), 1200−1100 (−C−C−).

**Synthesis of CdSe NCs.** CdSe NCs were synthesized following the procedures described in the literature.[32] An amount of 60 mg of CdO was mixed with 3 g of trioctylphosphineoxide (TOPO) along with 0.28 g of octadecylphosphonic acid. The mixture was stirred in $N_2$ atmosphere and heated to 300 °C. Then 1.5 g of trioctylphosphine (TOP) was carefully added and again heated to approximately 390 °C. The TOP-Se (1.7 mmol/mL) solution was then injected in to the mixed solution. The size of the NCs can be controlled by adjusting the reaction temperature and time. The synthesized NCs were carefully washed with toluene and methanol. The ligand exchange to pyridine was done by mixing the NCs in anhydrous pyridine and stirring at room temperature for overnight.

**Measurements.** A Bruker Advance-300 spectrometer was used to record $^1$H NMR and $^{19}$F NMR spectra. The thermal record was analyzed using a TA TGA 2100 thermogravimetric analyzer in a nitrogen atmosphere at a rate of 10 °C/min. Differential scanning calorimetry (DSC) measurement was conducted using a TA Instruments 2100 DSC apparatus with heating rate of 10 °C/min from 40 to 250 °C. Gel permeation chromatography (GPC) analysis was performed with polystyrene standard calibration (Waters high pressure GPC assembly model M515 pump, u-Styragel columns of


dx.doi.org/10.1021/am4007935 | ACS Appl. Mater. Interfaces 2013, 5, 6045−6053

HR4, HR4E, HR5E, with 500 and 100 Å, refractive index detectors, solvent THF) to determine molecular weights and polydispersity of the copolymers. UV−vis absorption spectra were recorded using a UV-1650PC spectrophotometer. Cyclic voltammetry (CV) was performed by using an EG and G Parc model 273 Å potentiostat/galvanostat system with a three electrode cell in a solution of 0.1 M tetrabutylammonium perchlorate ($Bu_4NClO_4$) in acetonitrile at a scan rate of 50 mV/s.

**Device Fabrication.** Bottom gate/top contact OTFTs were fabricated using conventional $Si^{2+}/SiO_2$ (300 nm) as a substrate. Cytop (AGC) was further deposited on the substrate to tune the dielectric surface to more hydrophobic one. (water contact angle > 108°) The thicknesses of the Cytop film was determined by using an ellipsometer (J. A. Woollam. Co. Inc.), to be ∼10 nm. The capacitance measurements were performed using an SR 720 LCR meter at frequencies ranging from 100 Hz to 100 kHz. The capacitance value measured at 100−120 Hz, 9.1 nF/cm$^2$ was used to extract the mobility. A thermally evaporated Au electrode (∼100 nm) was used as source-drain electrode to construct a 150 $\mu$m channel top contact, bottom gate OSCT. The transfer and output characteristics of the OSCT were measured in air using Keithley 2400 and 236 source/measure units.

OPVs were fabricated using the structure of ITO/PEDOT:PSS/conjugated polymer:$PC_{71}BM$/LiF/Al. After cleaning the prepatterned ITO-coated glass, the surface of the glass substrate was further modified by UV-ozone treatment for 20 min. As a buffer layer, poly(3,4-ethylenedioxythiophene)-polystyrenesulfonic acid (PEDOT:PSS) (Baytron PVP AI4083, Bayer AG) was spin-coated to a thickness of 30−50 nm and annealed at 120 °C (for 60 min) in air. $PC_{71}BM$ (99.5%) as the electron acceptor was obtained from NanoC. The various blend ratios of conjugated polymers to $PC_{71}BM$ (1:2 or 1:3 or 1:4 weight ratio) in chlorobenzene were prepared. The prepared solutions with concentration of 10 mg/mL were stirred in a nitrogen glovebox for 12 h. The active layer was spin-coated onto the PEDOT:PSS layer for 60 s to a thickness of 100 nm. Finally, lithium fluoride (LiF) (1 nm)/Al (100 nm) cathodes were thermally deposited. A Keithley 2400 source measurement unit was employed to obtain $I-V$ characteristics in the dark and under AM 1.5 G solar illumination (Zolix SS150A solar simulator) with respect to a reference cell PVM 132 calibrated at the National Renewable Energy Laboratory at an intensity of 100 mW/cm$^2$.

Photodetector was fabricated on conventional $Si^{2+}/SiO_2$ (300 nm) substrate. After cleaning, solutions containing the mixture of DTBDT-TTFO and CdSe NCs were spin-coated to form thin films with a nominal thickness of 100 nm. Finally, gold source and drain electrodes were evaporated on top of the semiconductor layers (60 nm) to build up coplanar geometry consisting of two gold electrodes and semiconductor. In all the measurements, typical channel widths ($W$) and lengths ($L$) were 1000 and 100 $\mu$m, respectively. Photocurrent was measured under illumination with the monochromatic light from a 150 W xenon arc lamp dispersed with a 1/8 m monochromator combined with LabView-controlled Keithley 2400 or 337 nm $N_2$ laser (6 ns duration) operated with function generator.

## RESULTS AND DISCUSSIONS

**Synthesis.** The synthesis routes of monomers and polymer are outlined in Scheme 1, and details are described in the Supporting Information. The monomers were obtained by manifold chemical reactions involving cycloannulation, reduction, oxidation, and nucleophilic addition. The TTFO monomer was synthesized by oxidation following a nucleophilic addition of heptadecafluorooctyl lithium and thieno[3,4-b]thiophene-2-carbaldehyde. The DTBDT was obtained by oxidation following a nucleophilic addition of benzo[1,2-b:4,5-b′]dithiophene-4,8-dione and 2,3-didecylthiophene. The new copolymer, DTBDT-TTFO, was synthesized by palladium-catalyzed Stille-coupling polymerization. The obtained polymer was purified by a Soxhlet method using methanol, acetone, hexane and chloroform. $^1$H NMR and IR analysis were performed to confirm the structure of the polymer. The polymer showed good solubility in common solvents, such as chloroform, THF, chlorobenzene and dichlorobenzene, due to its bulky dialkylthiophene side chains. GPC analysis provided a number-average molecular weight of 46.0 kDa with a polydispersity index (PDI) of 1.6.

**Thermal Analysis.** The thermogravimetric analyses (TGA) of DTBDT-TTFO revealed that a weight loss of 5% occurred at 354 °C, as shown in Figure 1a. The thermal transition

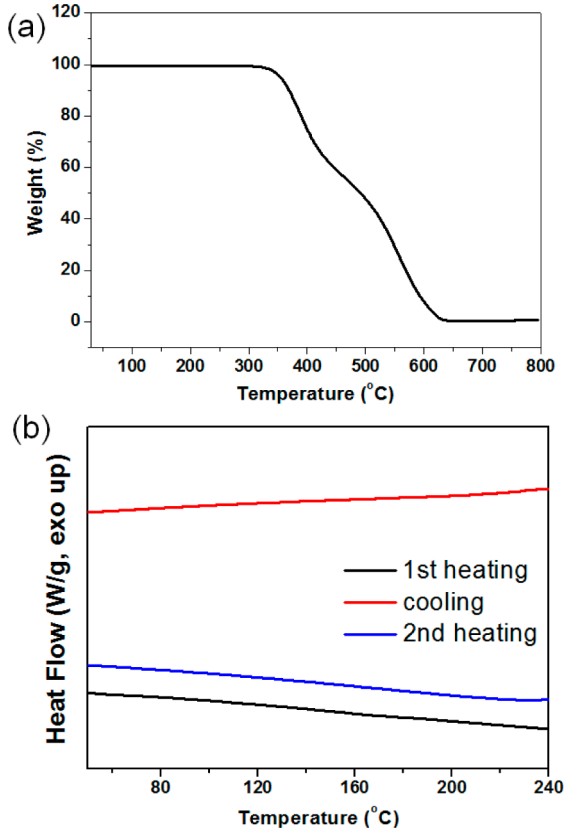


**Figure 1.** (a) TGA and (b) DSC analysis results of DTBDT-TTFO.

behaviors of the materials were also investigated using DSC, and the results are shown in Figure 1b. No notable transitions were observed throughout the measured temperature range, and those were reversible. From the thermal response, it can be concluded that DTBDT-TTFO is a low-crystalline polymer which is quite robust against thermal stress. X-ray diffraction on film of DTBDT-TTFO also suggests low crystalline nature (Figure S8, Supporting Information).

**Energy Level Analysis.** The UV−vis absorption spectra of DTBDT-TTFO as a solution in chloroform and as a film are shown in Figure 2a. Both reveal two major absorption peaks, which is a general feature of donor−acceptor type conjugated polymers. Interestingly, the absorption onset ($\lambda_{onset}$) of the polymer is fairly red-shifted compared to other derivatives of PBDTTT.[20,21] The $\lambda_{onset}$ value of DTBDT-TTFO is ∼1050 nm, which indicates a red-shift of ∼300 nm compared to those of other PBDTTT derivatives, leading to a dramatic decrease of the band gap to ∼1.2 eV. Note that previous works on PBDTTT derivatives showed that fluorinated thienothiophene resulted in only a lower HOMO level of the polymer, not a significant change of the bandgap. Here, the rather


dx.doi.org/10.1021/am4007935 | ACS Appl. Mater. Interfaces 2013, 5, 6045−6053

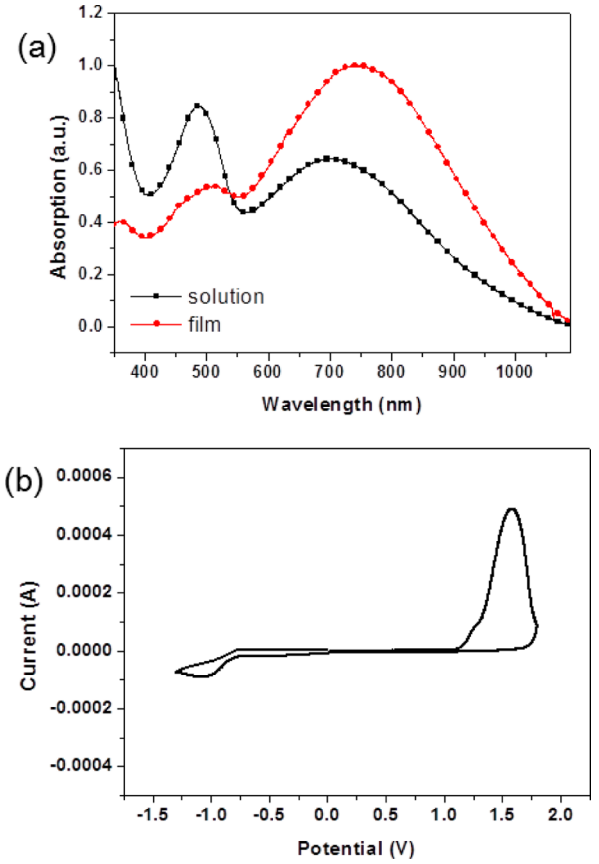


**Figure 2.** (a) UV−vis absorption spectra and (b) cyclic voltammetry spectra of DTBDT-TTFO.

unexpectedly low bandgap of the DTBDT-TTFO can be attributed to the very strong electron withdrawing effect of the perfluorinated alkylcarbonyl-substituted thieno-[3,4-b]-thiophene. In other words, the significantly strong electron withdrawing acceptor moiety of DTBDT-TTFO resulted in an exceptionally effective intramolecular charge transfer between the donor and acceptor units of DTBDT-TTFO. In this way, DTBDT-TTFO could extend its absorption range dramatically to the near-IR region, which is not the case with other PBDTTT derivatives with only slightly fluorinated thienothiophene.[16−18]

To check the effect of the perfluorinated thienothiphene moiety on the HOMO level of the polymer, cyclic voltammetry measurements (vs Ag/AgCl) were obtained for the DTBDT-TTFO, as shown in Figure 2b. The HOMO level can be estimated from the following equation: $E_{HOMO} = -E_{OX} - 4.4$ eV, where $E_{OX}$ is the onset of the oxidation potential, as determined by the intersection between two tangent lines. The calculated HOMO level is ∼5.6 eV, which is also lower than those of other PBDTTT derivatives. This finding can be clearly explained in terms of the effect of fluorine atoms with high levels of electron affinity. Considering the optical bandgap obtained previously, the resulting LUMO energy level of DTBDT-TTFO is ∼4.36 eV. Although one may expect a very high open-circuit voltage of OPVs based on DTBDT-TTFO from its low HOMO level, the LUMO energy level of DTBDT-TTFO, which is lower than that of PCBM, can ultimately limit the charge separation at polymer-PCBM interfaces, as discussed later.

**OTFT Characteristics.** Despite of the great success of PBDTTT derivatives in OPV applications, it is not easy to find examples of their applications to OTFTs. One example by Huo et al. reported that the charge carrier mobility of PBDTTT derivatives with a conjugated alkylthienyl side chain is higher than those with alkyl or alkoxy side chains based on the fabrication and analysis of OTFTs.[33] Here, we attempted to study the optimal performance of DTBDT-TTFO, which also has a thienyl-substituted side chain. To build an OTFT able to maximize the charge transport ability of DTBDT-TTFO, Cytop-treated $SiO_2$ (300 nm) was used as a dielectric layer, as Cytop is known to provide very hydrophobic interfaces for an upper deposited polymer layer, rather than conventional self-assembled monolayer. The resulting transfer and output characteristics of the OTFTs are shown in Figure 3. As shown

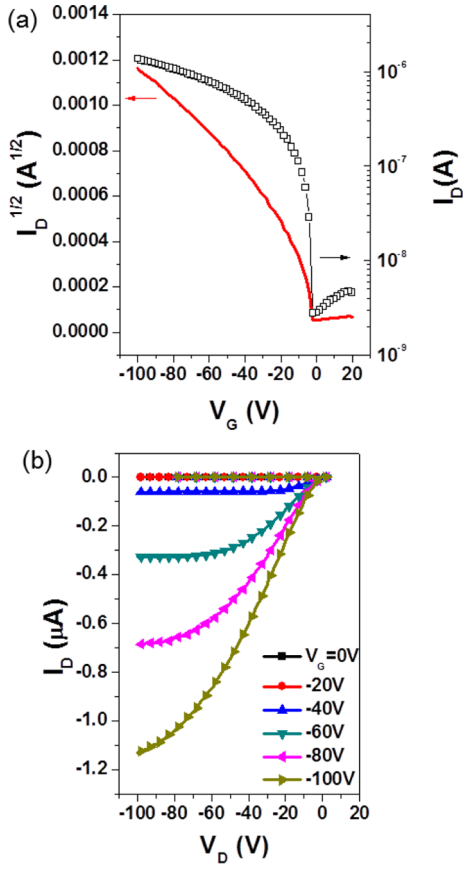


**Figure 3.** (a) Transfer and (b) output characteristics of OTFT based on DTBDT-TTFO.

in Figure 3a, typical transfer curves were obtained with the highest saturation mobility of 0.022 cm$^2$/(V s). The effect of thermal annealing on the mobility was not pronounced, reflecting the amorphous nature of the polymer. The output characteristics in Figure 3b show well-defined saturation behavior in the high voltage regime. However, in the low voltage regime, S-shaped behavior, which is known to be closely related to the contact resistance between the source electrode and the semiconductor, is observed as compared to well-defined linear behavior. Considering that the work function of Au is ∼5 eV,[34] such significant contact resistance is most likely due to the very deep HOMO level of DTBDT-TTFO, which generates a large energy barrier (∼0.6 eV) for carrier (hole) injection. Nonetheless, the measured mobility of 0.022 cm$^2$/(V


dx.doi.org/10.1021/am4007935 | ACS Appl. Mater. Interfaces 2013, 5, 6045−6053

s) is the highest among reported PBDTTT-based OTFTs. This result reveals the very successful charge transport ability of DTBDT-TTFO, originates from the enlarged delocalization of the $\pi$ electrons in the polymer backbone.

**OPV Characteristics.** In many of previous reports, PBDTTT derivatives showed great success in OPV applications with high PCE values exceeding 6%.[20,21] Such high performances as OPVs were attributed to the well matched energy levels of the polymer with respect to the PCBM as well as to their efficient light absorbing and charge transport abilities. Unfortunately, however, DTBDT-TTFO with an exceptionally low bandgap did not show satisfactory OPV performances with the conventional OPV device architecture. With the widely used ITO/PEDOT:PSS/BHJ/LiF/Al structure, the OPV performances were recorded under the AM 1.5 condition at 100 mW/cm$^2$. These results are summarized in Figure 4. The

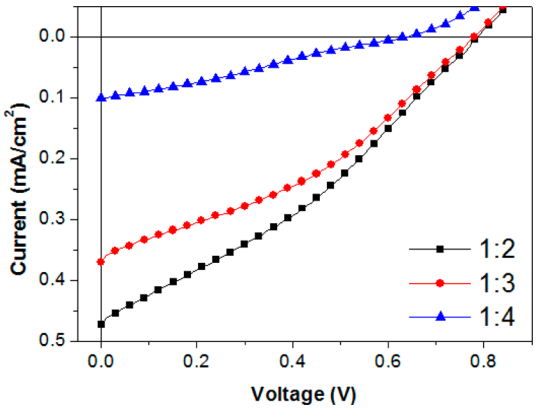


**Figure 4.** $I-V$ relations of OPV devices based on DTBDT-TTFO:PCBM BHJ under AM 1.5 condition at 100 mW/cm$^2$.

calculated PCE were only ~0.1%, mainly due to the extremely low short-circuit current. Generally, the LUMO level offset between the electron donor and acceptor is known to be the driving force for charge separation in a polymer:PCBM BHJ.[35,36] Therefore, in the BHJ of DTBDT-TTFO:PCBM, it seems reasonable to conclude that the lower LUMO level of the polymer (~4.36 eV) compared to that of the PCBM cannot guarantee charge separation at the donor−acceptor interface, resulting in a very OPV photocurrent. However, we still observed a high $V_{OC}$ of ~0.8 eV, which is higher than those of other previously reported PBDTTT derivatives, possibly originating from the rather deep HOMO level of DTBDT-TTFO.

**Photodetector Application.** Despite the unsuccessful performance of DTBDT-TTFO as OPV application, we can still expect alternative optoelectronic applications when considering its wide absorption range and high charge-carrier mobility. Here, we found that DTBDT-TTFO can serve behave as a good photodetector material when combined with low LUMO level-CdSe nanocrystal (NCs). Figure 5a shows the UV−vis absorption spectra of the synthesized colloidal CdSe NCs capped with TOPO ligands (thin film state), with the first exciton absorption maximum at approximately 600 nm. Figure 5b shows high resolution TEM images of the CdSe NCs, with a particle size of ~4 nm. The LUMO and HOMO energy levels of CdSe NCs (~4 nm) are approximately 4.3−4.5 and 6.2−6.3 eV, respectively.[37] Considering that the LUMO level position of DTBDT-TTFO is ~4.36 eV, CdSe NCs are a slightly better

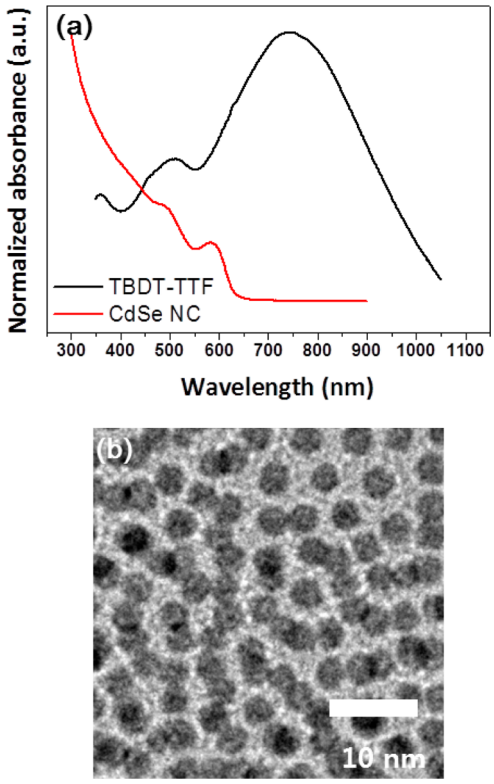


**Figure 5.** (a) UV−vis absorption spectra of CdSe NCs and (b) high resolution TEM image of CdSe NCs.

choice than PCBM for charge separation. To achieve efficient charge transfer between the polymer and the nanocrystals, we need to replace the insulating TOPO ligands with a shorter ligand. In this case, we used pyridine. A blended solution of DTBDT-TTFO:CdSe NCs with a weight ratio of 1:1 was used to fabricate the BHJ film.

Figure 6a shows the typical $I-V$ characteristics of the fabricated photoconductor under light exposure with various wavelengths. Considering the power at each wavelength of the light source used, the responsivity (A/W) was calculated as shown in Figure 6b. The highest responsivity of ~1 A/W is more than 1000 times higher than that of single component (DTBDT-TTFO only without NCs) devices with the same geometry. The relatively high photoresponse at 500 and 600 nm compared to that at 400 nm implies that photons absorbed by the polymer were more efficiently separated and thus contributed to the photocurrent gain. (Note that the charge carrier mobility of DTBDT-TTFO is apparently higher than CdSe NCs simply treated with pyrdine.) To the best of our knowledge, the responsivity of ~1 A/W is one of the highest values among all conducting polymer-based photodetectors, especially those operated at a low voltage (<1 V).[38−40] Figure 7a shows the TEM image of a representative hybrid film of DTBDT-TTFO and CdSe nanocrystals. The CdSe nanocrystals (darker region) are well dispersed in the polymer matrix without distinct aggregation of the nanocrystals or polymer domains. Such a homogeneous mixture between the donor and acceptor phases can promote exciton dissociating at the interface. Optical power dependence of responsivity (Figure 7b) in this device shows that the device is trap-limited and responsivity decreases with increasing optical power. In this paper, we have employed device structure of photoconductor. In this device, quite unique and useful is the effect of trapping,


dx.doi.org/10.1021/am4007935 | ACS Appl. Mater. Interfaces 2013, 5, 6045−6053

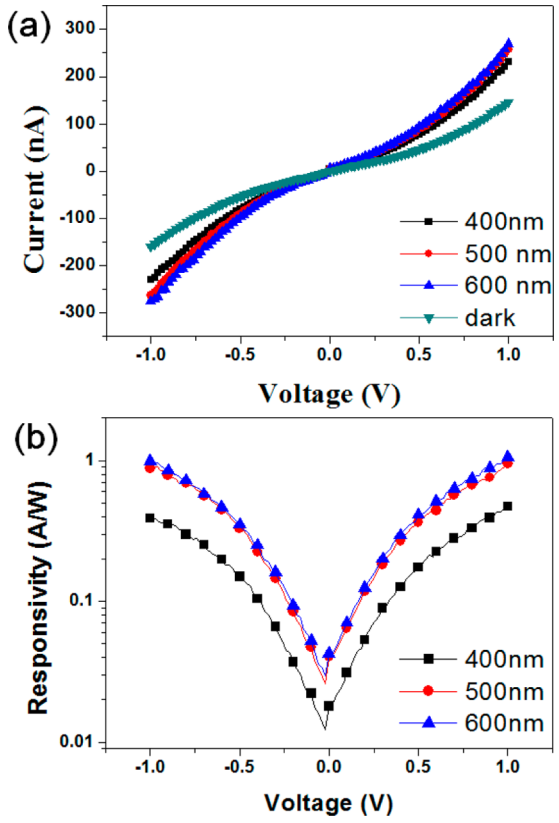


**Figure 6.** (a) $I-V$ relations and (b) responsivity-voltage relations of photodetector based on DTBDT-TTFO:CdSe NCs BHJ. Optical power: 1.74, 2.19, and 1.40 mW/cm$^2$ for 400, 500, and 600 nm of illuminated light, respectively.

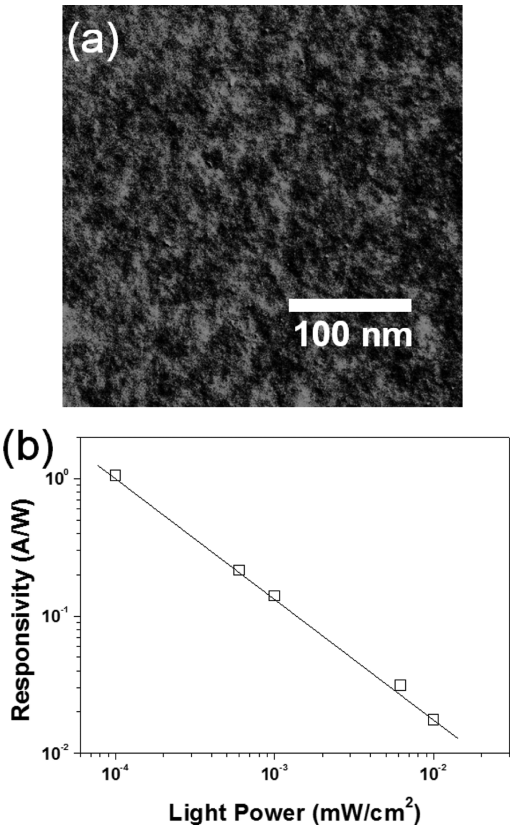


**Figure 7.** (a) TEM images of DTBDT-TTFO:CdSe NCs hybrids film. (b) Optical power dependence of responsivity of the photoconductor.

which can temporarily capture a charge (electron) but release it after some time. In our case, CdSe nanocrystals behave as trapping sites for electron because of lower electron mobility of organic-capped CdSe nanocrystal compared to hole mobility of polymer. Then the corresponding photogenerated hole will drift to the collecting electrode. The electron left behind makes charge unbalance in the system and lowers the potential for injection of hole to restore the charge neutrality in the material. The new hole injected in the system again moves to the collecting electrode because it has only small probability of encountering just trapped electron and recombining with it. In this way, the device obtains photoconductive gain until the trap states finally release the trapped electron. As intensity of illuminated light increases, the effective responsivity drops as a result of increasing probability of trap escaping. In such photoconductor, the gain is given as

$$G = cT\mu(E)V/L^2$$

where $c$ is the fraction of excitons that dissociate into trapped electrons and free holes, $\tau$ is the lifetime of the trapped electrons, $\mu(E)$ is the electric field-dependent hole mobility, $V$ is the applied voltage, and $L$ is the channel length. This equation clearly shows that the photocurrent gain depends strongly on both the ratio of charge dissociation and a high charge carrier mobility. In the case of DTBDT-TTFO/CdSe NCs hybrids, we conclude that homogeneous nanomorphology enabled high ratio of charge dissociation at the interface and high hole mobility of DTBDT-TTFO enabled successful circulation of holes, resulting in high photoresponsivity of >1 A/W.

The transient photocurrent response was also recorded, as shown in Figure 8. Regardless of the applied bias and wavelength of the light used, the photoresponse was quite prompt. To study the carrier lifetime in this device in more detail, photocurrent transients were obtained by illuminating the samples with a $N_2$ laser (337 nm, pulses with a duration of 6 ns) under 1 V of DC bias. The obtained temporal measurements of the photocurrent response revealed a main time constant of 120 $\mu$s and a faster component with a time constant of 5 $\mu$s. This suggests that the presence of some impurities or a TOPO ligand serves as a trapping species having an undesirably long-lived time constant of approximately120 $\mu$s. Note that the actual requirement in an imaging system for the photocurrent time constant of the detector is a few tens of milliseconds;[41] therefore, our DTBDT-TTFO:CdSe NCs photodetector can perform fairly well with lag-free operation. Furthermore, the results here imply that with the optimized ligand treatment, the upper bound of the response speed of the photodetector would correspond to a time constant of 5 $\mu$s.

## CONCLUSION

A new low-bandgap PBDTTT derivative, DTBDT-TTFO, was synthesized, and various optoelectronic applications of DTBDT-TTFO were demonstrated. In particular, the synthesized DTBDT-TTFO showed an unpredicted low LUMO level, which is not adequate in OPV applications due to the difficulty related to charge separation at the polymer−PCBM interface. However, the DTBDT-TTFO:CdSe NCs BHJ showed fairly successful charge separation, as proved by a high performance

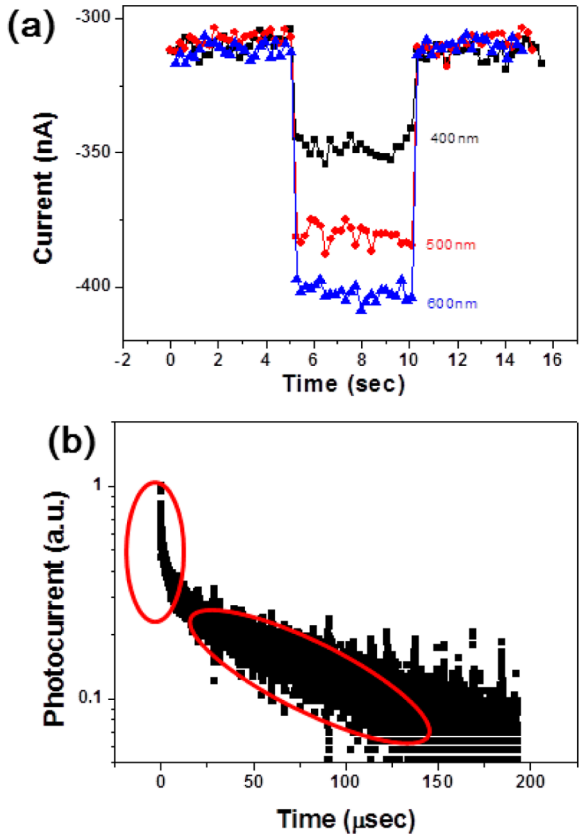


**Figure 8.** Transient photocurrent measurements of the photodetector at the time scale of (a) a few seconds and (b) a few microseconds. Red circle in (b) indicates two representative time regimes calculated for time scale.

photodetector. The optimized photodetector resulted in high responsivity of 1A/W under a low operating voltage (<1 V) as well as high speed operation corresponding to a time scale of a few hundreds of $\mu$-seconds. Such high performance as a photodetector was attributed to the high charge carrier mobility of the DTBDT-TTFO (0.02 $cm^2/(V\ s)$) and to the successful charge trapping ability of the CdSe NCs.

## ■ ASSOCIATED CONTENT

### Supporting Information

Additional details as described in the text. This material is available free of charge via the Internet at http://pubs.acs.org.

## ■ AUTHOR INFORMATION

### Corresponding Author

*E-mail: dchung@cau.ac.kr (D.S.C.); ykim@gnu.ac.kr (Y.-H.K.); skwon@gnu.ac.kr (S.-K.K.)

### Notes

The authors declare no competing financial interest.

## ■ ACKNOWLEDGMENTS

This research was supported by the Basic Science Research Program through the National Research Foundation of Korea (NRF), and by ministry of Education, Science and Technology (Grant number: 201206047047). And this work was supported by the New and Renewable Energy Technology Development Program of (KETEP) grant funded by the Ministry of Knowledge Economy (No. 20113020010070) and NAP National Agenda Project Program (NAP-08-1).

## ■ REFERENCES

(1) McCulloch, I.; Ashraf, R. S.; Biniek, L.; Bronstein, H.; Combe, C.; Donaghey, J. E.; James, D. I.; Nielsen, C. B.; Schroeder, B. C.; Zhang, W. *Acc. Chem. Res.* **2012**, *45*, 714−722.
(2) Li, G.; Zhu, R.; Yang, Y. *Nat. Photonics* **2012**, *6*, 153−161.
(3) Li, Y. *Acc. Chem. Res.* **2012**, *45*, 723−733.
(4) Bian, L.; Zhu, E.; Tang, J.; Tang, W.; Zhang, F. *Prog. Polym. Sci.* **2012**, *37*, 1292−1331.
(5) Park, J. W.; Lee, D. H.; Chung, D. S.; Kang, D. M.; Kim, Y.-H.; Park, C. E.; Kwon, S.-K. *Macromolecules* **2010**, *43*, 2118−2123.
(6) Sirringhaus, H.; Tessler, N.; Friend, R. H. *Science* **1998**, *280*, 1741−1743.
(7) Sirringhaus, H.; Kawase, T.; Friend, R. H.; Shimoda, T.; Inbasekara, M.; Wu, W.; Woo, E. P. *Science* **2000**, *290*, 2123−2126.
(8) Sirringhaus, H.; Brown, P. J.; Friend, R. H.; Nielsen, M. M.; Bechgaard, K.; Langeveld-Voss, B. M. W.; Spierlng, A. J. H.; Janssen, R. A. J.; Meijer, E. W.; Herwig, P.; de Leeuw, D. M. *Nature* **1999**, *401*, 685−688.
(9) Ong, B. S.; Wu, Y.; Liu, P.; Gardner, S. *Adv. Mater.* **2005**, *17*, 1141−1144.
(10) Mcculloch, I.; Heeney, M.; Bailey, G.; Genevicius, K.; Macdonald, I.; Shkunov, M.; Sparrowe, D.; Tierney, S.; Wagner, R.; Zhang, W.; Chabinyc, M. L.; Kline, R. J.; Mcgehee, M. D.; Toney, M. F. *Nat. Mater.* **2006**, *5*, 328−333.
(11) Kronemeijer, A. J.; Gili, E.; Shahid, M.; Rivnay, J.; Salleo, A.; Heeney, M.; Sirringhaus, H. *Adv. Mater.* **2012**, *24*, 1558−1565.
(12) Chen, H.; Guo, Y.; Yu, G.; Zhao, Y.; Zhang, J.; Gao, D.; Liu, H.; Liu, Y. *Adv. Mater.* **2012**, *24*, 4618−4622.
(13) Kang, I.; An, T. K.; Hong, J.; Yun, H.-J.; Kim, R.; Chung, D. S.; Park, C. E.; Kim, Y.-H.; Kwon, S.-K. *Adv. Mater.* **2013**, *25*, 524−528.
(14) Ma, W.; Yang, C.; Gong, X.; Lee, K.; Heeger, A. J. *Adv. Funct. Mater.* **2005**, *15*, 1617−1622.
(15) Irwin, M. D.; Buchholz, D. B.; Hains, A. W.; Chang, R. P. H.; Marks, T. J. *Proc. Natl. Acad. Sci. U.S.A.* **2008**, *105*, 2783−2787.
(16) Kim, J. Y.; Kim, S. H.; Lee, H.-Ho; Lee, K.; Ma, W.; Gong, X.; Heeger, A. J. *Adv. Mater.* **2006**, *18*, 572−576.
(17) Peet, J.; Kim, J. Y.; Coates, N. E.; Ma, W. L.; Moses, D.; Heeger, A. J.; Bazan, G. C. *Nat. Mater.* **2007**, *6*, 497−500.
(18) Liang, Y.; Feng, D.; Wu, Y.; Tsai, S.-T.; Li, G.; Ray, C.; Yu, L. *J. Am. Chem. Soc.* **2009**, *131*, 7792−7799.
(19) Zhang, Z.-G.; Zhang, S.; Min, J.; Cui, C.; Geng, H.; Shuai, Z.; Li, Y. *Macromolecules* **2012**, *45*, 2312−2320.
(20) Chen, H.-Y.; Hou, J.; Zhang, S.; Liang, Y.; Yang, G.; Yang, Y.; Yu, L.; Wu, Y.; Li, G. *Nat. Photonics* **2009**, *3*, 649.
(21) Son, H. J.; Wang, W.; Xu, T.; Liang, Y.; Wu, Y.; Li, G.; Yu, L. *J. Am. Chem. Soc.* **2011**, *133*, 1885−1894.
(22) Huang, Y.; Guo, X.; Liu, F.; Huo, L.; Chen, Y.; Russell, T. P.; Han, C. C.; Li, Y.; Hou, J. *Adv. Mater.* **2012**, *24*, 3383−3389.
(23) Li, G.; Zhu, R.; Yang, Y. *Nat. Photonics* **2012**, *6*, 153−161.
(24) Padinger, F.; Rittberger, R. S.; Sariciftci, N. S. *Adv. Funct. Mater.* **2003**, *13*, 85−88.
(25) Bao, Z.; Dodabalapur, A.; Lovinger, A. J. *Appl. Phys. Lett.* **1996**, *69*, 4108−4110.
(26) Chen, L. M.; Xu, Z.; Hong, Z. R.; Yang, Y. *J. Mater. Chem.* **2010**, *20*, 2575−2598.
(27) Lee, K.; Kim, J. Y.; Park, S. H.; Kim, S. H.; Cho, S.; Heeger, A. J. *Adv. Mater.* **2007**, *19*, 2445−2449.
(28) Gilot, J.; Barbu, I.; Wienk, M. M.; Janssen, R. A. J. *Appl. Phys. Lett.* **2007**, *91*, 113520.
(29) Park, J. H.; Seo, Y. G.; Yoon, D. H.; Lee, Y.-S.; Lee, S.-H.; Pyo, M.; Zong, K. *Eur. Polym. J.* **2010**, *46*, 1790−1795.
(30) Yoon, M.-H.; Di Benedetto, S.; Matthew, A.; Russell, T.; Facchetti, A.; Marks, T. J. *Chem. Mater.* **2007**, *19*, 4864−4881.
(31) Huo, L.; Hou, J.; Zhang, S.; Chen, H. Y.; Yang, Y. *Angew. Chem., Int. Ed.* **2010**, *49*, 1500−1503.
(32) Peng, Z. A.; Peng, X. J. *Am. Chem. Soc.* **2001**, *123*, 183−184.
(33) Huo, L.; Zhang, S.; Guo, X.; Xu, F.; Li, Y.; Hou, J. *Angew. Chem., Int. Ed.* **2011**, *50*, 9697−9702.

(34) Bao, Z.; Locklin, J. *Organic Field-Effect Transistors*; CRC Press: New York, 2006.
(35) Ohkita, H.; Cook, S.; Astuti, Y.; Duffy, W.; Tierney, S.; Zhang, W.; Heeney, M.; McCulloch, I.; Nelson, J.; Bradley, D. D. C.; Durrant, J. R. *J. Am. Chem. Soc.* **2008**, *130*, 3030−3042.
(36) Clarke, T.; Ballantyne, A.; Jamieson, F.; Brabec, C.; Nelson, J.; Durrant, J. *Chem. Commun.* **2009**, 89−91.
(37) Yang, J.; Tang, A.; Zhou, R.; Xue, J. *Sol. Energ. Mat. Sol. C* **2011**, *95*, 476−482.
(38) Campbell, I. H.; Crone, B. K. *J. Appl. Phys.* **2007**, *101*, 024502-1−024502-5.
(39) Chen, H. Y.; Lo, M. K. F.; Yang, G.; Monbouquette, H. G.; Yang, Y. *Nat. Nanotechnol.* **2008**, *3*, 543−547.
(40) Gong, X.; Tong, M. H.; Xia, Y. J.; Cai, W. Z.; Moon, J. S.; Cao, Y.; Yu, G.; Shieh, C. L.; Nilsson, B.; Heeger, A. J. *Science* **2009**, *325*, 1665−1667.
(41) Konstantatos, G.; Sargent, E. H. *Proc. IEEE* **2009**, *97*, 1666−1683.